Hindawi Publishing Corporation
Journal of Applied Mathematics
Volume 2014, Article ID 726205, 18 pages
http://dx.doi.org/10.1155/2014/726205

Research Article

Stepped Fault Line Selection Method Based on Spectral Kurtosis and Relative Energy Entropy of Small Current to Ground System

Xiaowei Wang, Xiangxiang Wei, Jie Gao, Yaxiao Hou, and Yanfang Wei

School of Electrical Engineering and Automation, Henan Polytechnic University, Jiaozuo 454000, China

Correspondence should be addressed to Xiaowei Wang; proceedings@126.com

Received 9 April 2014; Revised 8 June 2014; Accepted 8 June 2014; Published 22 July 2014

Academic Editor: Hamid R. Karimi

This paper proposes a stepped selection method based on spectral kurtosis relative energy entropy. Firstly, the length and type of window function are set; then when fault occurs, enter step 1: the polarity of first half-wave extremes is analyzed; if the ratios of extremes between neighboring lines are positive, the bus bar is the fault line, else, the SK relative energy entropies are calculated, and then enter step 2: if the obtained entropy multiple is bigger than the threshold or equal to the threshold, the overhead line of max entropy corresponding is the fault line, if not, enter step 3: the line of max entropy corresponding is the fault line. At last, the applicability of the proposed algorithm is presented, and the comparison results are discussed.

1. Introduction

Most of 3~66 kV distribution networks are so-called small current to ground system in china, which includes unearthed neutral system, arc suppression coil compensated neutral system, and high resistance-grounded neutral system. Since the fault current is small and the arc is unstable instability, suitable fault line selection methods are lacking [1, 2].

When fault occurs, the researchers are attracted by the rich transient fault features. At present, the main research methods are based on the transient fault signal, such as Wavelet transform [3, 4], S transform [5, 6], Prony algorithm [7], Hilbert-Huang transform (HHT) [8, 9], and correlation analysis [10, 11]. In [3, 4], the transient zero-sequence current (TZSC) is decomposed by wavelet, and the transient energy is calculated; according to the differences, the fault line is selected, when the high grounding resistance fault occurs, which can lead to misjudgment because of the compensation of arc suppression coil to the TZSC. Good time frequency of S transform can be used to select fault line; in [5, 6], the dominant frequencies of TZSC are obtained by S transform, which are used as the selection criterions; however, there is much information after S transform, and what should be further studied is how to take advantage of the phase angles. Prony algorithm can fit the low frequency transient signal well; in [7], Prony is used to fit the TZSC to select the dominant components, and then the relative entropy of dominant components is obtained to select the fault line, but what should be further studied is how to determine the model orders. In [8, 9], HHT is used to decompose the TZSC, and then the most high-frequency component of the intrinsic mode functions (IMF) can be obtained, and based on this, the selection criterion is built; however, the decomposition process may cause modal aliasing. In [10, 11], the poor waveform similarity of the TZSC between the fault line and the healthy line is noticed, and the coefficients are obtained to select the fault line; however, when the small-angle fault occurs, the similarity of the TZSC that flows the healthy cable line and the healthy overhead lines gets worse.

Aiming at few features that are available in arc suppression coil to ground system, single fault line selection method is not very reliable, and this paper regards the ratios of the first half-wave extremes between neighboring lines and spectral kurtosis (SK) relative energy entropy as features to select the fault line, a stepped fault line selection method is proposed by utilizing two kinds of features. When fault occurs, enter step 1, and if the ratios of first half-wave extremes between neighboring lines are positive, the bus bar is selected as the fault line, and the line selection process is done. Otherwise, the SK relative energy entropies of branch lines are computed,

then enter step 2, if the obtained entropy multiple is greater than or equal to the threshold, the overhead line is judged as the fault line, and the overhead line of max entropy corresponding is selected as the fault line, and the fault line selection process is done. If the entropy multiple is less than the threshold, enter step 3, and the line of max entropy corresponding is selected as the fault line.

The remaining of this paper is organized as follows. In Section 2, characteristics of TZSC are presented. In Section 3, basic theories about spectral kurtosis and wavelet denoising are presented. In Section 4, feasibility analysis of spectral kurtosis algorithm is presented. In Section 5, basic theories about fault line selection are presented. In Section 6, fault line selection criterions are proposed. In Section 7, simulation and verification are presented. In Section 8, applicability analysis is presented. In Section 9, two kinds of comparison results are discussed. In Section 10, the paper is completed with conclusions and future directions.

2. Characteristics of TZSC

Zero sequence equivalent circuit of single phase to ground is shown in Figure 1, C_0 and L_0 are the zero-sequence equivalent capacitance and inductance, respectively, R_g is the ground transition resistance, R_p and L_p are the equivalent resistance and inductance of arc suppression coil, respectively, and $G(t)$ is the zero-sequence voltage.

From Figure 1, the TZSC $i_0(t)$ through the fault point is

$$i_0(t) = i_{0L}(t) + i_{0C}(t) = I_{Lm}\cos\varphi e^{-t/\tau_L} + I_{Cm}\left(\frac{\omega_f}{\omega}\sin\varphi\sin\omega t - \cos\varphi\cos\omega_f t\right)e^{-\delta t}, \quad (1)$$

$i_{0L}(t)$ and $i_{0C}(t)$ are the inductor and capacitive current, respectively, I_{Lm} and I_{Cm} are the initial value of $i_{0L}(t)$ and $i_{0C}(t)$, respectively, ω is the angular frequency, ω_f and δ are the angular frequency of free oscillations and the attenuation coefficient, respectively, and $\delta = 1/\tau_c$, τ_c is the decay time constant of $i_{0C}(t)$, τ_L is the decay time constant of $i_{0L}(t)$, and φ is the initial phase of the fault line [12].

From (1), $i_{0L}(t)$ and $i_{0C}(t)$ make up the fault TZSC, both of which include nonperiodic damped component and stable periodic component. At beginning, τ_L is greater than τ_c; therefore, $i_{0L}(t)$ is deteriorated slower than $i_{0C}(t)$.

It can be known from the above analysis that the TZSC is mutant signal when fault occurs, and as time goes on, it would decrease gradually. Considering the good frequency-domain effect for unstable, nonperiodic, mutant, and damped signal of SK, SK algorithm is introduced to extract the feature information of TZSC in this paper.

3. Basic Theories

3.1. Definition of SK. Kurtosis is random 4-order cumulative amount and cannot reflect specific signal changes as a global index; therefore, kurtosis is improper to detect the signal with strong noise. In order to overcome the weakness of kurtosis, SK is proposed by Immovilli et al. [13–15].

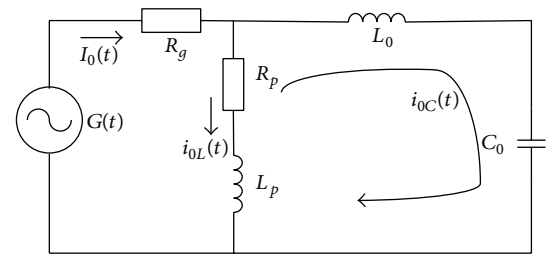

Figure 1: Zero sequence equivalent circuit.

$x(t)$ is decomposed by Wold-Cramer under the nonstationary condition, and the result is as follows:

$$Y(t) = \int_{-\infty}^{+\infty} e^{j2\pi ft} H(t,f)\, dX(f), \quad (2)$$

$H(t, f)$ is the complex envelope at frequency f of $Y(t)$, and also $H(t, f)$ changes with time. In a practical system, $H(t, f)$ is random, $X(f)$ is the strict white noise spectrum, and ω is random with time varying of filter.

Fourth-order spectrum cumulant of $Y(t)$ can be defined as follows:

$$C_{4Y}(f) = S_{4Y}(f) - S^2{}_{2Y}(f) \quad (f \neq 0), \quad (3)$$

$S_{2nY}(f)$ is the $2n$ moments, which can be defined as follows:

$$S_{2nY}(f) \triangleq \frac{E\left\{\left|H(t,f)\, dX(f)\right|^{2n}\right\}}{df}. \quad (4)$$

Therefore SK can be defined as follows:

$$K(f) \triangleq \frac{C_{4Y}(f)}{S^2_{2Y}(f)} = \frac{S_{4Y}(f)}{S^2_{2Y}(f)} - 2, \quad (f \neq 0). \quad (5)$$

The important properties of SK are as follows.

(1) The SK of pure stationary process is –1, $f \neq 0$.

(2) The SK of a stationary Gaussian process is 0.

The TZSC $i_0(t)$ can be expressed as follows:

$$i_0(t) = Y(t) + b(t), \quad (6)$$

$Y(t)$ is the actual TZSC and $b(t)$ is the noise. $Y(t)$ and $b(t)$ are independent; therefore, the SK of $i_0(t)$ is

$$K_{(x+b)}(f) = \frac{K_x(f)}{\left[1 + \rho(f)\right]^2}, \quad (7)$$

$\rho(f) = (S_b(f)/S_{i_0}(f))$ is the ratio of noise to signal, and $S_b(f)$ and $S_{i_0}(f)$ are power spectral densities of $b(t)$ and $Y(t)$, respectively.

It can be known from (7) that $K_{(x+b)}(f) \approx K_{i_0}(f)$ when $\rho(f)$ is very small and $K_{(x+b)}(f) \approx 0$ when $\rho(f)$ is very

large. So the SK can search the whole frequency band, and the characteristic frequency bands can be detected easily.

3.2. SK Based on Short-Time Fourier Transforms (STFT). $i_0(n)$ is the discrete form of $i_0(t)$, $n = 1, 2, \ldots, N$, and the calculation of SK based on STFT is as follows:

$$Y_w(kP, f) = \sum_{n=1}^{N} i_0(n)\, w(n - kP)\, e^{-j2\pi nf}, \tag{8}$$

$w(n)$ is the window function, whose length is N_w, P is the time step, and k is the number of time steps.

The $2n$-order spectrum distance of $Y_w(kP, f)$ is defined as follows:

$$S_{2nY} = \left\langle \left| Y_w(kP, f) \right|^{2n} \right\rangle_k, \tag{9}$$

$\langle \cdot \rangle_k$ is k-order time average.

Considering the definition of SK in Section 3.1, when $n = 1$ and $n = 2$, based on STFT, and SK can be described as follows [16]:

$$K(f) = \frac{S_{4Y}(f)}{S_{2Y}^2(f)} - 2. \tag{10}$$

It can be seen that the $i_0(t)$ can be characterized by SK based on STFT, and the frequency band of the max SK corresponding can be obtained finally.

3.3. Basic Principle of Wavelet Denoising

3.3.1. Basic Principle of Wavelet Transform. The basis function of the wavelet transform can be defined as follows [17, 18]:

$$\psi_{u,v}(t) = \frac{1}{\sqrt{u}} \psi\left(\frac{t - v}{u}\right) \quad u > 0,\ v \in R, \tag{11}$$

where u is the scale parameters and v is the translation parameter.

The continuous wavelet transform of $\psi(t)$ is a function defined as

$$\mathrm{WT}_f(u, v) = \langle f, \psi_{u,v} \rangle = \frac{1}{\sqrt{u}} \int_R f(t)\, \overline{\psi}\left(\frac{t - v}{u}\right) dt. \tag{12}$$

In order for an inverse wavelet transform to exist, the mother wavelet $\psi(t)$ should satisfy the admissibility condition: $C_\psi = \int_R (|\psi(\widehat{\omega})|^2 / |\omega|) d\omega < +\infty$ ($\psi(\widehat{\omega})$ is the complex conjugate of $\psi(t)$). So $\psi(t)$ is an admissible wavelet. Choosing admissible wavelet, the original signals are reconstructed by

$$f(t) = \frac{1}{C_\psi} \int \int_R \mathrm{WT}_f(u, v) \cdot \left[\frac{1}{\sqrt{u}} \psi\left(\frac{t - v}{u}\right)\right] \frac{1}{u^2} du\, dv. \tag{13}$$

In practice, u and v must be discrete. Let $u = u_0^m$ and $v = nv_0u_0^m$, and (13) can be presented as

$$\psi_{m,n}(t) = u_0^{-m/2} \psi\left(u_0^{-m} t - nv_0\right). \tag{14}$$

Function family $\{\psi_{m,n}(t), m, n \in Z\}$ is called discrete wavelet. When $u_0 = 2$ and $v_0 = 1$, function family $\{\psi_{m,n}(t)\}$ constructs a group orthonormal basis on which signals can be reconstructed.

3.3.2. Process of Wavelet Denoising. The basic principle of wavelet denoising is based on the spectrum distribution characteristics of signals and noise. According to the principle, noise of each decomposition level is eliminated, and useful signal is preserved [19, 20].

The substance of denoising is restraining the unwanted signal and boosting the useful signal. The one-dimensional K_i ($i = 1, 2, \ldots, N_w$) can be expressed as follows:

$$K_i = f_i + \varepsilon e_i, \tag{15}$$

K_i is the observable SK with noise, f_i is the real SK without noise, e_i is the gauss random signal, and ε is the standard deviation of noise.

The denoising process of one-dimensional signals can be divided into three steps.

Step I. Mother wavelet function and the levels of decomposition are determined, and then K_i can be decomposed by wavelet transform.

Step II. High frequency coefficients are processed by the threshold.

The threshold thr is

$$\mathrm{thr} = \sigma \sqrt{2 \log_e(N_w)}, \tag{16}$$

where σ is the standard deviation of K_i and N_w is the length of K_i.

Step III. Signals can be reconstructed by adding the low-frequency coefficients and high frequency coefficients, and the result is K_i'.

4. Feasibility Analysis of Spectral Kurtosis Algorithm

The ideal signal is defined to show the SK algorithm characteristics, and the details are as follows:

$$\begin{aligned}
i_0(n) &= i_{01}(n) + i_{02}(n) + i_{03}(n) + i_{04}(n) + \varepsilon(n), \\
i_{01}(n) &= 5.6 \cos\left(2\pi \times 50t + \frac{\pi}{3}\right), \\
i_{02}(n) &= 40e^{-56t} \cos\left(2\pi \times 250t + \frac{\pi}{6}\right), \\
i_{03}(n) &= 72e^{-102t} \cos(2\pi \times 315t), \\
i_{04}(n) &= 10e^{-5.5t},
\end{aligned} \tag{17}$$

where $i_{01}(n)$ is the fundamental frequency component, $i_{02}(n)$ is the 5th harmonic component, $i_{03}(n)$ is noninteger harmonic component, $i_{04}(n)$ is the decaying direct current (DC) component, $\varepsilon(n)$ is gauss white noise signal, and SNR $= -13.5$ dB.

The ideal TZSC $i_0(n)$ is a nonperiodic signal, added by $i_{01}(n)$, $i_{02}(n)$, $i_{03}(n)$, $i_{04}(n)$, and $\varepsilon(n)$; what should be noted is

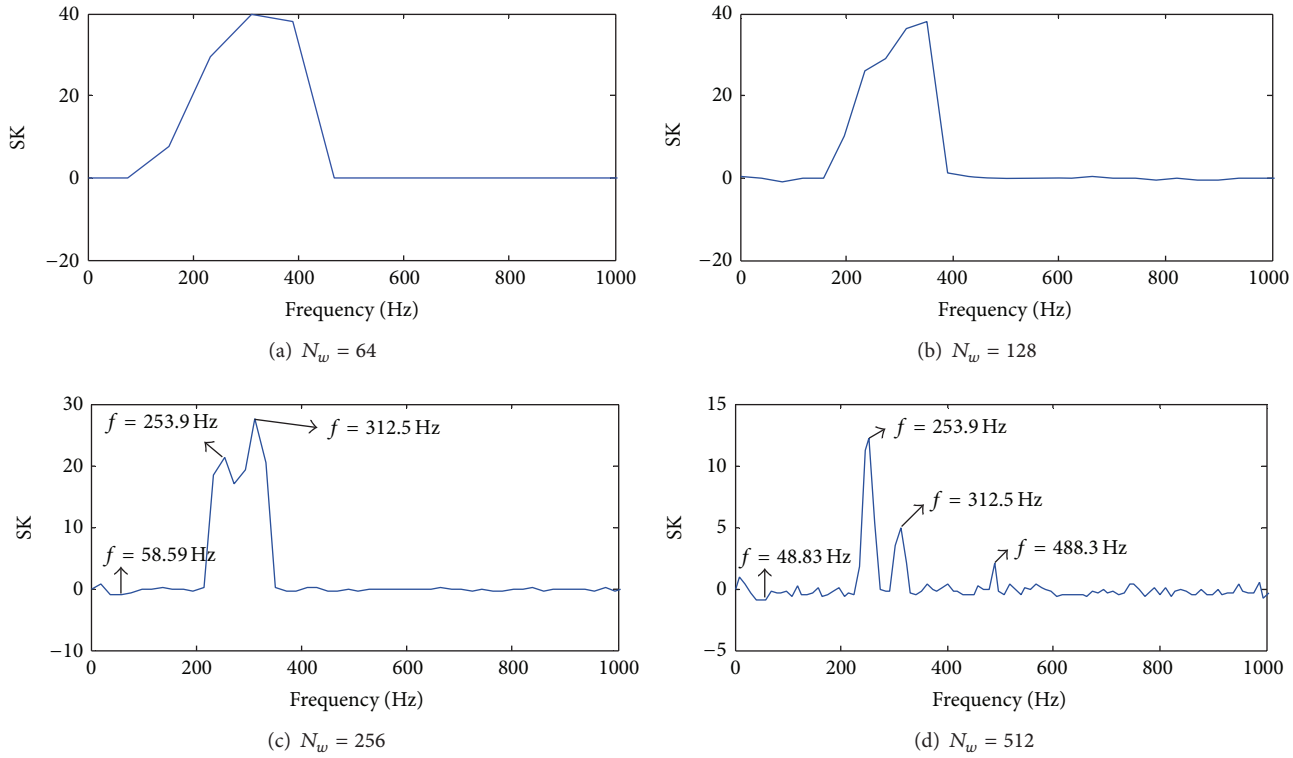

Figure 2: Length of window function.

that the ideal signal is generated according to the features of the TZSC [21, 22].

4.1. Set the Length of Window Function. The sampling frequency f_c = 10000 HZ, the simulation time is 0.6 s, and SK algorithm is used to analyze the ideal TZSC. The adjacent frequency interval is $f_c/2N_w$, as N_w are 64, 128, 256, and 512, and the frequency intervals are 78.13 Hz, 39.06 Hz, 19.53 Hz, and 9.77 Hz, respectively. The results of SK based on STFT are shown in Figure 2.

As Figure 2 shows, different lengths of window function make a difference for SK. When N_w is 64 or 128, to a certain extent, the ideal TZSC can be characterized; however, the frequency resolution is lower, fundamental frequency is not imprecise, and the 5th harmonic signal cannot be characterized. When N_w is 256, frequency resolution meets the requirements, and three types of signal frequency can be distinguished, because of the interval between adjacent SK. The frequency f causes errors, and the results are f = 58.59 Hz, f = 253.9 Hz, and f = 312.5 Hz. When N_w is 512, frequency resolution is higher, and fundamental frequency is more accurate; however, SK contains much noise; for example, as Figure 2(d) shows, f = 488.3 Hz belongs to spurious frequency components.

4.2. Set the Type of Window Function. After the length of window function is determined, the window functions are selected, such as Gaussian window (gausswin), Hamming window, Hanning window, and Kaiser window. Based on the SK algorithm, the results are shown in Figure 3.

It is known from Figure 3 that different window functions can also characterize the TZSC's frequency, and the SK of white noise is close to 0. Therefore, the types of window function have a little impact on the SK. Because of being less effective than other window functions, Kaiser should avoid being used.

In conclusion, SK algorithm can distinguish the frequency components of the TZSC. In order to extract the features more perfectly, Hanning window is selected in this paper, whose length is 256.

5. Basic Theories about Fault Line Selection

5.1. Steps of Denoising. The calculation process of SK can be interfered by various noise; firstly, wavelet analysis is introduced to eliminate the noises, whose frequency is approximate to the frequency of TZSC's SK K_i ($i = 1, 2, \ldots, N_w$), since symlets wavelet are limited compactly supported wavelets and whose local capabilities in the time domain and frequency domain are good, considering SK algorithm has good local capabilities in the frequency domain, and the frequency characteristic of sym6 is good, whose frequency resolution can also meet the requirements. White noise belongs to a stationary random interference signal; according to the properties (2) in Section 3.1, the SK of white noise is 0, but the defects from the outside condition make the SK of white noise fluctuate around 0. Finally, the threshold method is proposed to correct SK, which can also eliminate the effects

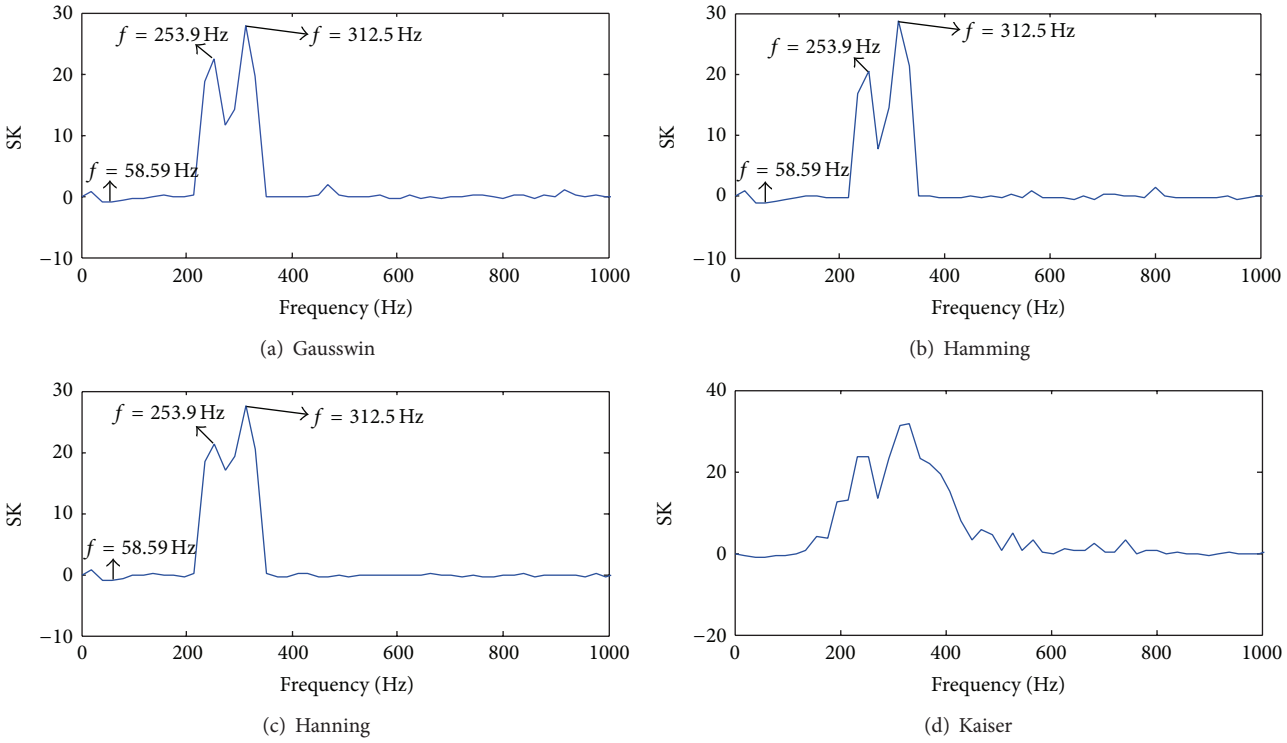

Figure 3: Types of window function.

on the SK relative energy entropy caused by the white noise. Specific processes are as follows.

(1) K_i is decomposed into 4 layers by sym6.

(2) Soft threshold process the high frequency coefficients of each decomposition scale in Section 3.3.2 Step II.

(3) Reconstruct one-dimensional wavelet by adding the bottom of the low frequency coefficients and high frequency coefficients, and the result is K_i'.

(4) The waveform correction coefficient λ is introduced, and the equation is

$$\xi = \lambda \cdot K'_{\max}, \quad 0 \le \lambda \le 1, \tag{18}$$

where $K'_{\max}$ is the max K_i', and considering the value relation between K_i' and $K'_{\max}$, the coefficient λ is 20% in the paper.

(5) K_i' is retained the same value as long as $K_i' \ge \xi$; otherwise, $K_i' = 0$, the result is $\widehat{K}_i$.

After wavelet denoising and threshold correcting, the noise in $\widehat{K}_i$ decreases significantly, and a premise of calculating the SK relative energy entropy is accurately provided.

5.2. The SK Relative Energy Entropy. In information theory, entropy represents uncertainty of average information and can also be used to estimate the complexity of random signals, it provides useful information about underlying the dynamic processes of signal, SK algorithm can magnify a local frequency characteristic of the TZSC, and small and short abnormalities are found in the frequency domain by SK energy entropy. The impact of fault conditions mainly reflected on time-frequency distribution of the TZSC [23–25], in order to reflect the changes of SK in the frequency domain, based on the relative entropy and energy entropy, and the SK relative energy entropy C_j is defined in the paper:

$$C_j = -\sum_{i=1}^{N_w} u_{ji} \log_2 u_{ji}, \quad j = 1, 2, \ldots, l, \tag{19}$$

where u_{ji} is the SK relative energy probability distribution, $u_{ji} = \widehat{K}_{ji}^2 / E_{\max}$, $E_{\max} = \max(E_j)$, $E_j = \sum_{i=1}^{M} \widehat{K}_{ji}^2$, the number of overhead lines is l_1, and the SK relative energy entropies are C_a $(a = 1, 2, \ldots, l_1)$. The number of hybrid lines and cable lines is l_2, and the SK relative energy entropies are C_b $(a = 1, 2, \ldots, l_2)$.

It can be known from the above definition that C_j is the information entropy that the SK energy of line j is relative to the max energy of all lines, the SK relative energy probability distributions are based on the sum of the largest SK energy, the probability space of SK energy is united, u_{ji} is a relative quantity, which has a unique sensitivity for the change of output frequency, and C_j can describe the relative uniformity for SK energy distribution in the frequency domain.

6. Fault Line Selection Criterions

In [26], it can be known from the simulation waveforms that the sign of first half-wave extremes between the fault branch

line and the healthy branch lines is opposite. However, the signs of first half-wave extremes among the branch lines are the same when the bus bar fault occurs. According to this, the criterion of bus bar fault is obtained.

6.1. Step 1—The Bus Bar Fault Criterion

(1) The first half-wave extremes i_{0zj} of branch lines are recorded when fault occurs, and then the ratios G_{0zm} of i_{0zj} are calculated:

$$G_{0zm} = \frac{i_{0zj}}{i_{0z(j+1)}}, \quad m = 1, 2, \ldots, l-1. \tag{20}$$

(2) If $G_{0zm} > 0$, the bus bar is selected as the fault line, and the selection process is done; otherwise, the following steps should be executed.

6.2. Step 2 and Step 3—The Branch Lines Fault Criterions. The distributed complexity and uncertainty of the TZSC are reflected by the energy entropy in the frequency domain [27]; when fault occurs, the SK relative energy entropy reflects the amount of information that can be used to select the fault line. Because of the interaction between the overhead lines and cable lines, the line with the max relative energy entropy may be not the fault line; in order to avoid the influence, the relative energy of the overhead line and cable line, hybrid line would be compared in this paper, respectively.

The entropy multiple β is introduced to judge the overhead line fault, and the calculation process is as follows:

$$\beta = \frac{C_{a\max}}{C_{as\max}}, \quad \beta \geq 1, \tag{21}$$

where $C_{a\max}$ is the max of C_a and $C_{as\max}$ is the second biggest of C_a. After a number of simulations, the threshold of entropy multiple β is set to 2 in this paper.

When the branch line fault occurs, firstly, enter step 2, judge whether the overhead line is fault or not, according to (21), calculate β, if $\beta \geq 2$ is satisfied, the overhead line of $C_{a\max}$ corresponding is selected when the fault line is selected, and the selection process is done. Otherwise, enter step 3, the hybrid line or cable line of $C_{b\max}$ corresponding is selected as the fault line, and the selection process is done.

The specific selection flowchart is shown in Figure 4.

7. Simulation and Verification

In this paper, the ATP-EMTP is used to simulate a single phase-to-ground fault, and the simulation model is shown in Figure 5, there are 4 lines (S_1, S_2, S_3 and S_4).

The parameters of simulation model are as follows.

Overhead line positive-sequence parameters are $R_1 = 0.17\,\Omega$/km, $L_1 = 1.2$ mH/km, and $C_1 = 9.697$ nF/km, and zero-sequence parameters are $R_0 = 0.23\,\Omega$/km, $L_0 = 5.48$ mH/km, and $C_0 = 6$ nF/km.

Cable line positive-sequence parameters are $R_{11} = 0.193\,\Omega$/km, $L_{11} = 0.442$ mH/and km, $C_{11} = 143$ nF/km, and zero-sequence parameters are $R_{00} = 1.93\,\Omega$/km, $L_{00} = 5.48$ mH/and km, $C_{00} = 143$ nF/km.

Transformer is 110/10.5 kV, the leakage impedance of high voltage is $(0.40 + j12.20)\,\Omega$, the leakage impedance of low voltage is $(0.006 + j0.183)\,\Omega$, excitation current is 0.672 A, magnetizing flux is 202.2 Wb, and magnetic resistance is 400 kΩ. Load is all are delta, $Z_L = 400 + j20\,\Omega$, and arc suppression coil is $L_N = 1281.9$ mH, $R_N = 40.2517\,\Omega$.

When the overhead line S_1 fault occurs, the initial fault angle is 0° and the grounding resistance is 50 Ω, and the TZSC waveforms are shown in Figure 6.

As Figure 6 shows, the TZSC is mutant when fault occurs, then they are damped. The conclusions are consistent with the analysis about the characteristics of the TZSC in Section 2; therefore, SK algorithm is introduced to analyse the fault information contained in the TZSC, and the characteristic frequency bands can be selected.

Table 1: First half-wave extremes.

Overhead line S_1	Overhead line S_2	Hybrid line S_3	Cable line S_4
178.7320	−15.0541	−72.0865	−149.6746

7.1. Select Based on Step 1. The first half-wave extremes i_{0zj} of $i_{0j}(t)$ ($j = 1, 2, 3, 4$) are obtained when fault occurs, and the results are in Table 1.

Because $i_{0z1}/i_{0z2} = 178.7320/(-15.0541) = -11.8726 < 0$, according to step 1, it can be known that the bus bar is healthy in the power distribution system. In order to select the fault line, step 2 is needed.

7.2. Select Based on Steps 2 and 3. The definition of characteristic frequency f_T is the frequency f that the max SK $K_{\max}$ is corresponding in the specific condition.

According to the above analysis of SK algorithm in Section 4, Hanning window is selected, whose length is 256. And then K_i are calculated, the results are in Figure 7 (SNR = −5.5623 dB), considering too high frequency without actual physical meaning, and only the frequency of SK below 10000 Hz is listed in this paper.

The following conclusions are obtained from Figure 7.

(1) Several different frequency components in the TZSC can be contained. For example, two kinds of different frequency within 2000 Hz are contained in S_2 at least.

(2) Because of the flaws of SK algorithm and the impact of auxiliary white noise, the values of SK are fluctuant around 0, which are not equal to the theoretical value 0.

(3) Different frequency components of the transient zero sequence current signals are amplified by SK; among them, the most prominent frequency components are $f_T = 781.3$ Hz for S_1, because the amplitude of SK in 781.3 Hz is larger than any other amplitude of SK. Similarly, the most prominent frequency components are $f_T = 390.6$ Hz for S_2, the most prominent frequency components is $f_T = 585.9$ Hz for S_3, and

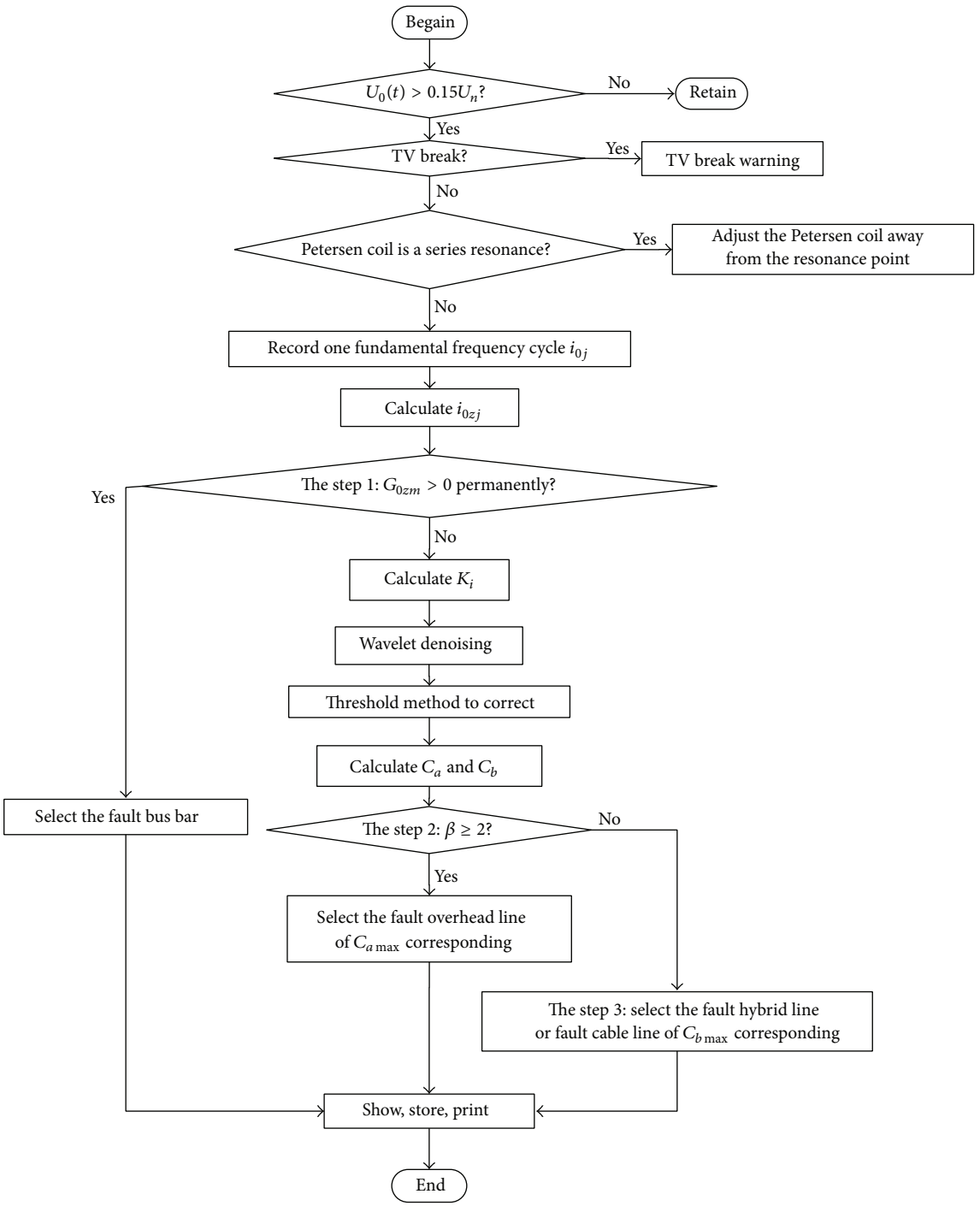

Figure 4: Flowchart of fault line selection.

the most prominent frequency components is f_T = 585.9 Hz for S_4.

The conclusion (3) shows that the characteristic frequency f_T of fault line is larger than the f_T of healthy line in this fault condition. Therefore calculate SK of each branch line, and try to select the fault line by observing the characteristic frequency f_T directly [2]. According to the SK algorithm, f_T can be obtained with different initial angles θ and grounding resistances R, Hanning window is selected, whose length is 256, SNR = −5.5623 dB, and the results are shown in Table 2.

The following conclusions can be obtained from Table 2.

(1) S_1 is the fault line, and f_T of S_1 is larger than the f_T of S_2, and f_T between S_3 and S_4 are either equal or close.

(2) Since the inductance of the cable lines is less far than the inductance of overhead lines, the capacitance to

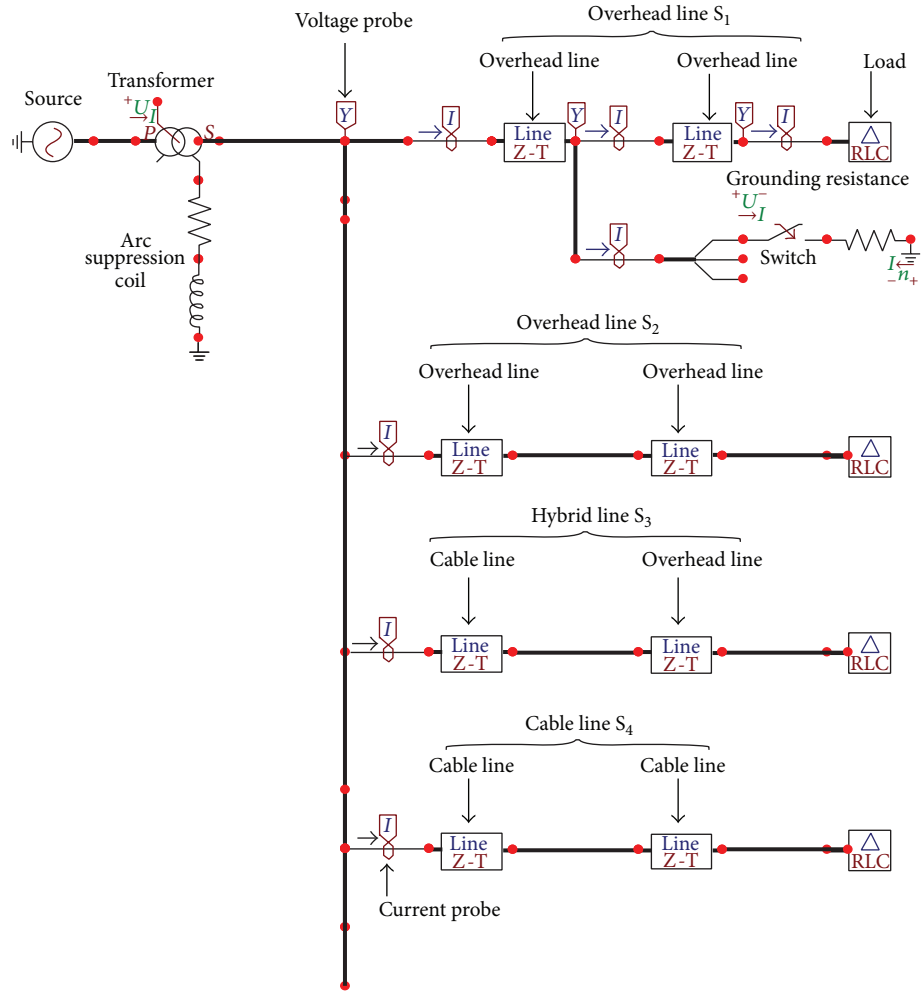

Figure 5: Arc suppression coil grounding system.

Table 2: f_T of each line with S_1 fault.

Initial angle θ	Grounding resistance R/Ω	Characteristic frequency f_T (Hz)			
		Overhead line S_1	Overhead line S_2	Hybrid line S_3	Cable line S_4
0°	20	585.9	390.6	585.9	585.9
	200	3320	2344	3320	3125
150°	20	585.9	390.6	585.9	585.9
	200	3320	2344	3320	3125

ground of the cable lines is larger several times than the latter, the parameter of cable lines can make a difference in the spectral characteristics of TZSC [28], and it shows that the f_T of fault overhead line S_1 is either equal or close to S_3 and S_4.

(3) When S_1 is fault, the initial phase angle θ is from 0° up to 150° and the grounding resistance R is fixed. The f_T of same line is unchanged; however, if the grounding resistance R is from 20 Ω up to 200 Ω and the initial phase angle θ fixed, the f_T of S_1 is from 585.9 Hz up to 3320 Hz, and the f_T of S_2 is from 390.6 Hz up to 2344 Hz. In conclusion, the initial phase angle θ has little effect on f_T, but the grounding resistance has great effect on the f_T, because of the effect of the grounding resistance making the f_T nonunique.

It can be seen that the f_T would be nonunique with different resistances; therefore, the healthy line and the fault line cannot be distinguished only by f_T,. Considering that the more obvious of the fault features are, the larger difference of entropy between the healthy line and fault lines is, so the SK relative energy entropy is introduced to distinguish the fault line and the healthy lines in this paper.

To eliminate the noises, whose frequency is approximate to the frequency of K_i, wavelet analysis is introduced to

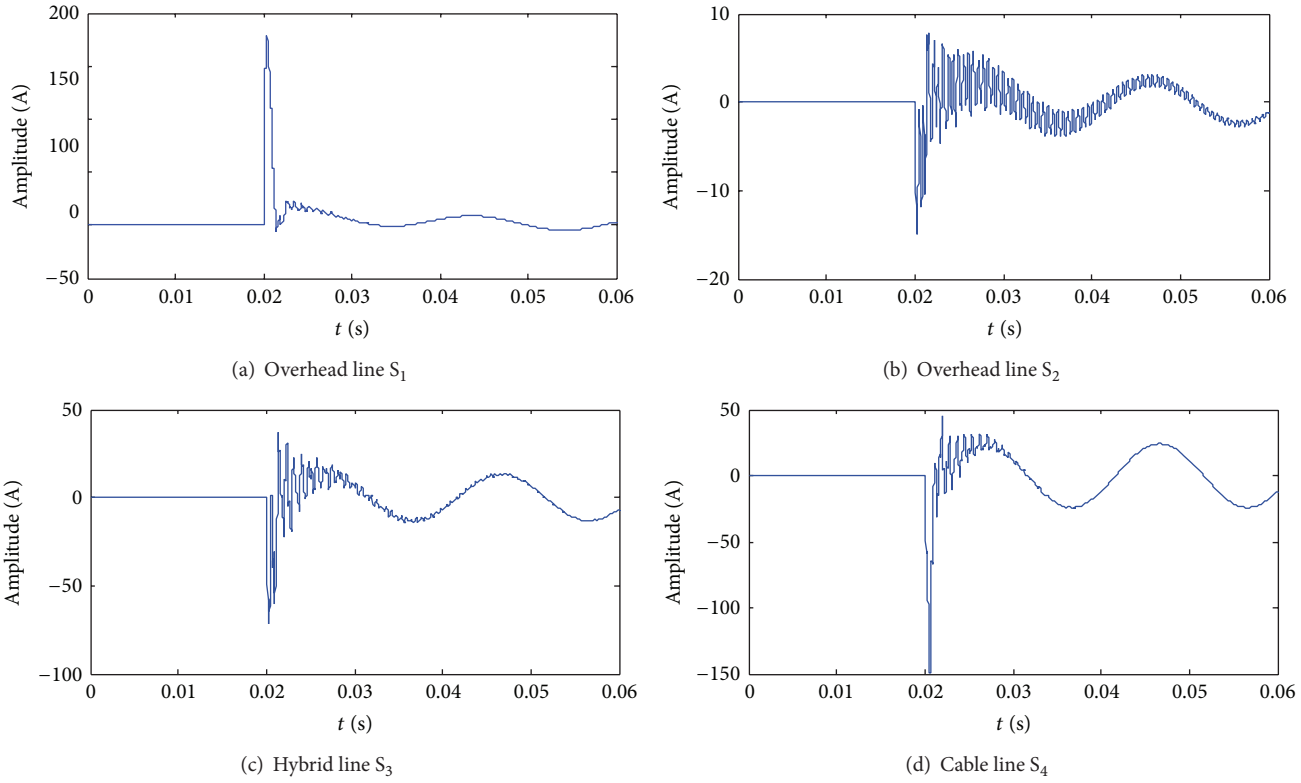

Figure 6: Transient zero-sequence current.

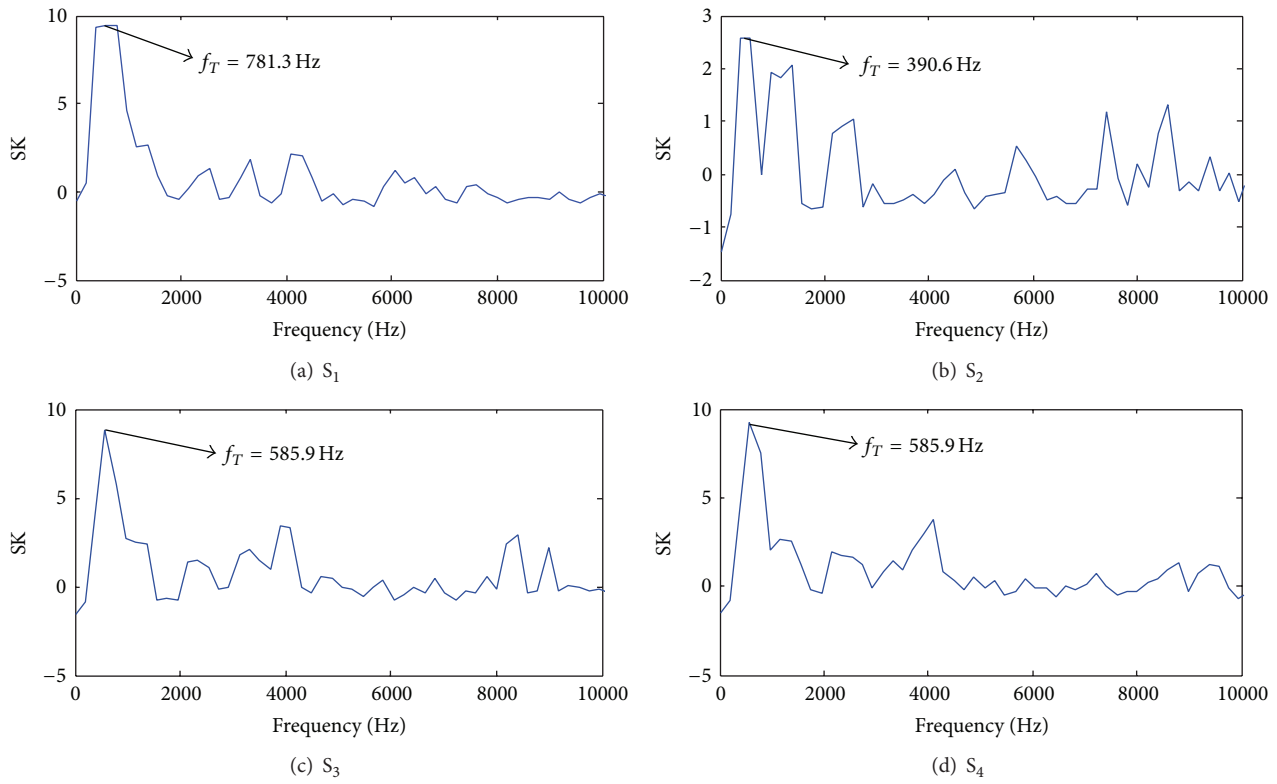

Figure 7: Corresponding f_T of SK.

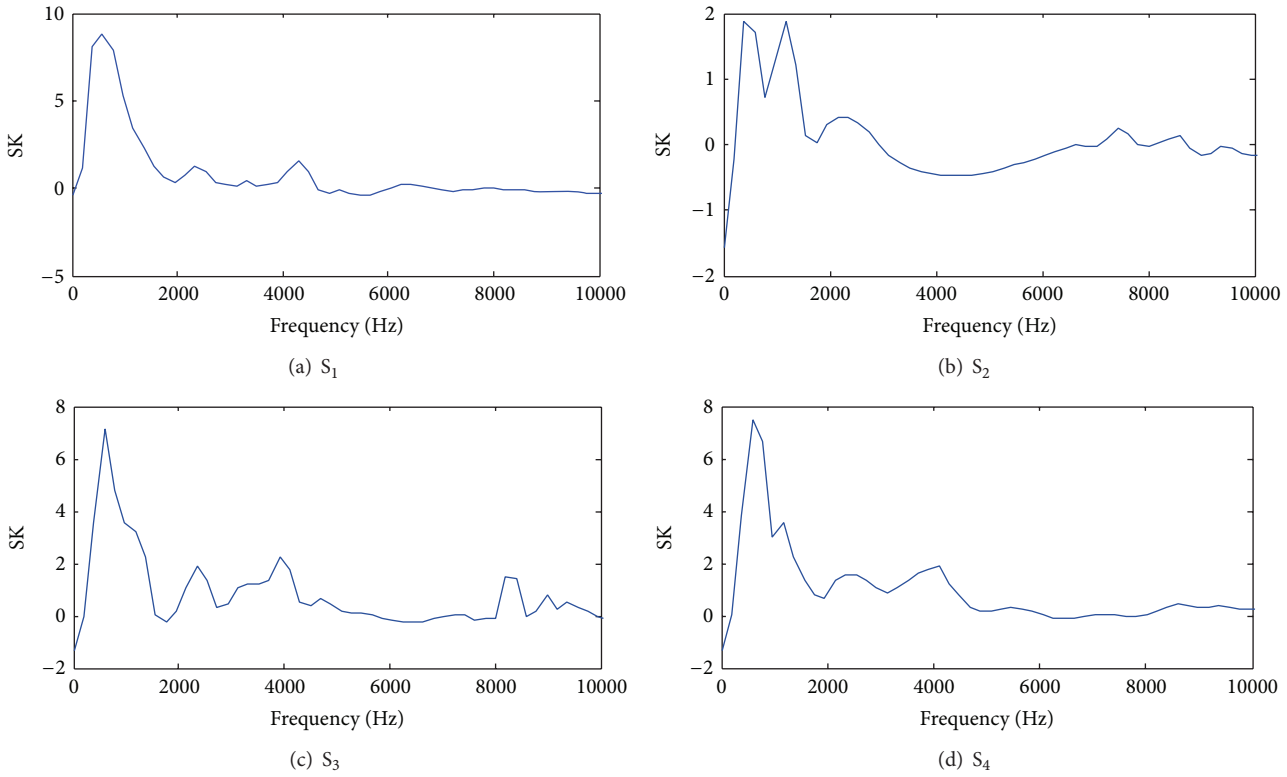

Figure 8: Denoising spectral kurtosis.

Table 3: SK relative energy entropy.

Branch line	S_1	S_2	S_3	S_4
C_j	2.2788	0.9179	1.6239	2.2834

denoising before calculating the relative energy entropy, and the results are in Figure 8.

From Figure 8, the noise signals decrease obviously after denoising, the values of SK fluctuate around 0 in the high frequency (over 5000 Hz), the waveforms are more smoothly, and the result is K_i'.

To decrease the interference from the SK of white noise to the SK relative energy entropy of TZSC, the threshold method is introduced to correct K_i' in this paper, and the finally results $\widehat{K}_i$ are shown in Figure 9.

From Figure 9, most of the frequencies are below 5000 Hz in $\widehat{K}_j$, and the SK of white noise is set to 0 artificially by the threshold method actually. The results show that the effect of white noise is decreased, and a premise that calculates C_j accurately is provided. The results are in Table 3.

Based on the fault line selection method of step 2, according to (21), calculate β, $\beta = C_{a\max}/C_{as\max} = 2.2788/0.9179 = 2.48 > 2$ is satisfied, although C_4 is larger than C_1, C_2, and C_3, in view of $\beta > 2$, and S_1 is selected as the fault line.

For S_1 belongs to the overhead line, it can be known that the bus bar is healthy after step 1, then enter step 2, calculate β, $\beta > 2$ is satisfied, and therefore S_1 is judged as the fault line without step 3.

7.3. Results of Different Fault Types. To verify the accuracy of the proposed stepped fault line selection method further, the results are given when the bus bar fault occurs, the overhead line is S_1, the hybrid line is S_3, and the cable line is S_4 with different θ and R.

7.3.1. Bus Bar Fault. When the bus bar fault occurs with different initial phase angles θ and grounding resistances R, according to step 1, the selection results are in Table 4.

When the bus bar fault occurs, it can be known from Table 4 that R, θ would make a difference for i_{0zj}, which can be described as the larger R is, the lower i_{0zj} is, i_{0zj} is from negative to positive when θ is from 0° up to 150°, and the absolute value of i_{0zj} decreases. When $\theta = 0°$, $i_{0zj} < 0$ is satisfied; however, when $\theta = 150°$, $i_{0zj} > 0$ is satisfied, the conclusion that whatever R and θ change, $G_{0zm} > 0$ is right permanently, the criterion of bus bar fault are satisfied. Therefore, the fault bus bar can be selected by step 1, the theory of bus bar fault selection method is simple, the results are correct and credible, and the influence from R and θ is avoided.

7.3.2. Overhead Line Fault in S_2. When the overhead line S_2 fault occurs with different θ and R, according to step 1 and step 2, the selection results are in Table 5, phase A to grounding

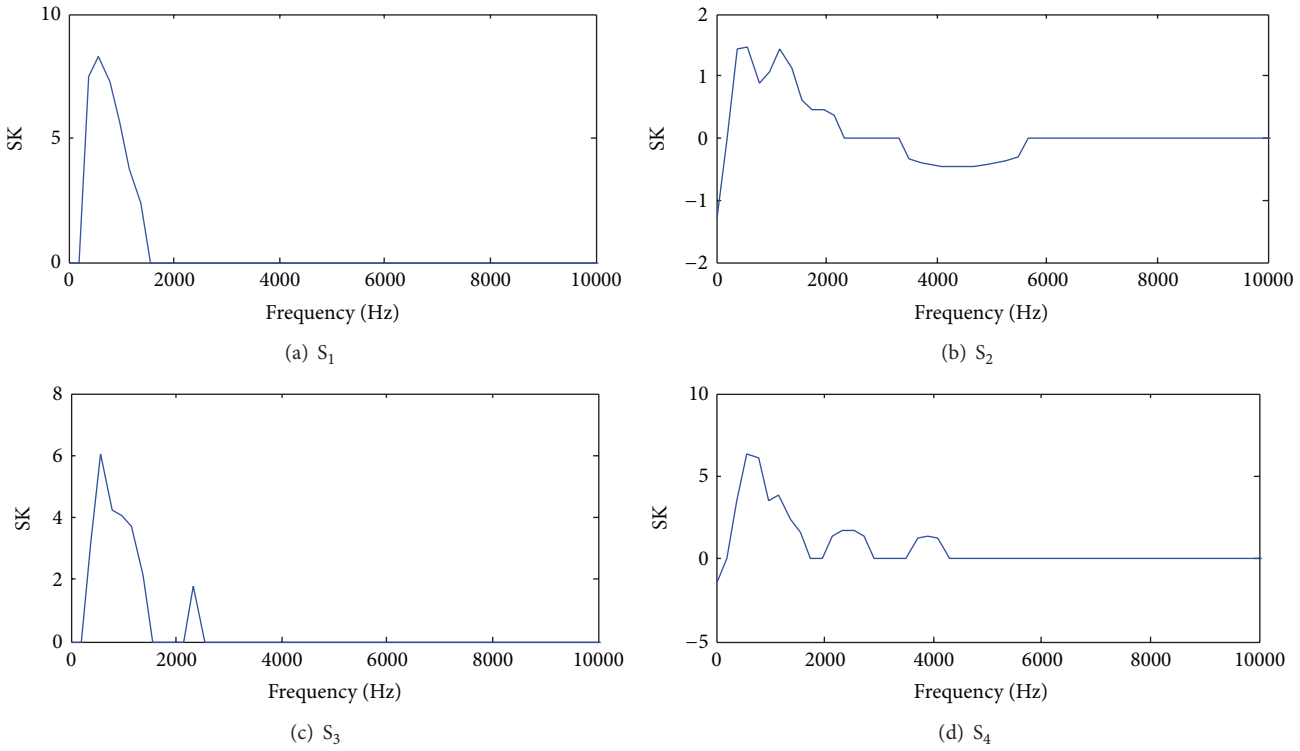

Figure 9: Revising spectral kurtosis.

Table 4: First half extremes of the TZSC with bus bar faults.

Fault line	θ	R/Ω	First half extremes of TZSC i_{0zj}				$G_{0zm} > 0$?	Results
			S_1	S_2	S_3	S_4		
Bus bar	0°	20	−36.7519	−23.2945	−157.7988	−229.0609	Y	Bus bar
		200	−9.7630	−8.8730	−35.6166	−68.9971	Y	Bus bar
	150°	20	22.1604	20.3579	98.0850	150.7914	Y	Bus bar
		200	6.0437	5.8571	23.0452	44.5919	Y	Bus bar

Table 5: SK relative energy entropy with S_2 fault.

Fault line	θ	R/Ω	SK relative energy entropy C_j				Entropy multiple β	Results
			S_1	S_2	S_3	S_4		
Overhead line S_2	0°	20	0.5324	3.9787	1.8911	2.4950	7.47 > 2	S_2
		200	1.1521	4.4164	3.5851	3.2250	3.83 > 2	S_2
	150°	20	0.5761	2.9607	2.2864	2.2134	5.14 > 2	S_2
		200	2.9918	7.0234	7.8605	5.0687	2.35 > 2	S_2

fault occurs, and the fault location is 5 km away from the bus bar.

From Table 5, the SK relative energy entropy of fault line is larger than the healthy lines in most cases. According to step 2, calculate β, because of $\beta = C_{a\ \max}/C_{as\ \max} \geq 2$, the overhead line is judged as fault line preliminary, because C_2 belongs to the $C_{a\ \max}$, S_2 is selected as the fault line finally, and the selection results are accurate without step 3. When the overhead line fault occurs, the results show that utilizing the stepped fault line selection method to select the fault line only to enter step 1 and step 2, and without step 3. The selection process is simplified.

From the results of Tables 4 and 5, the fault line selection method not only ensures the accuracy of fault line selection but also can save the time of fault line selection by steps 1 and 2. Besides, the fault line selection method cannot be influenced by R and θ.

7.3.3. Hybrid Line S_3 and Cable Line S_4 Fault. When the hybrid line S_3 or cable line S_4 fault occurs with different θ

Table 6: SK relative energy entropy with S_3 and S_4 faults.

Fault line	θ	R/Ω	SK relative energy entropy C_j				Entropy multiple β	Results
			S_1	S_2	S_3	S_4		
Hybrid line S_3	0°	20	1.4287	1.5408	4.9297	4.8318	1.08 < 2	S_3
		200	1.0894	1.1655	3.5634	2.8949	1.07 < 2	S_3
	150°	20	1.1355	1.1165	4.4099	3.8247	1.02 < 2	S_3
		200	0.7395	0.4809	3.5649	2.1245	1.54 < 2	S_3
Cable line S_4	0°	20	0.8222	0.7218	3.7140	5.1669	1.14 < 2	S_4
		200	1.7250	1.1495	2.5230	4.0801	1.50 < 2	S_4
	150°	20	0.4447	0.4522	3.3416	4.1139	1.02 < 2	S_4
		200	2.8497	4.0614	3.1244	3.6334	1.43 < 2	S_4

Table 7: SK relative energy entropy with different fault distances ($\theta = 0°$, $R = 20\,\Omega$).

Fault line	SK relative energy entropy C_j				Entropy multiple β	Results
	S_1	S_2	S_3	S_4		
Overhead line S_1	2.7267	1.2616	2.1665	2.8215	2.16 > 2	S_1
Cable line S_4	1.6140	1.1455	3.9845	4.3558	1.41 < 2	S_4

Table 8: SK relative energy entropy with different fault phases ($\theta = 0°$, $R = 20\,\Omega$).

Fault line	Fault phase	SK relative energy entropy C_j				Entropy multiple β	Results
		S_1	S_2	S_3	S_4		
Overhead line S_1	B	3.0161	1.3442	1.7646	2.9313	2.24 > 2	S_1
	C	2.1819	0.4247	1.0312	1.4207	5.14 > 2	S_1
Cable line S_4	B	0.6462	0.7357	3.5225	5.2236	1.14 < 2	S_4
	C	2.0681	3.6244	1.2483	1.4300	1.75 < 2	S_4

and R, respectively, according to steps 1, 2, and 3, phase A to ground fault occurs, the fault location is 5 km away from the bus bar, and the stepped fault line selection results are in Table 6.

From Table 6, according to steps 1 and 2, calculate β, because of $\beta = C_{a\,\max}/C_{as\,\max} < 2$, the fault line belongs to S_3 or S_4 preliminary, then step 3 is needed, the line of $C_{b\,\max}$ corresponding is selected as the fault line, the fault line S_3 or S_4 can be selected after step 3 finally. From the above, the fault hybrid line or the fault cable line can be selected accurately after steps 1, 2, and 3.

8. Applicability Analyses

8.1. Different Fault Distances. To verify the proposed method adaptability with different fault distances, θ and R are fixed, and the simulations are as follows. Taking the fault line S_1 and S_4 as examples, the fault locations are 10 km and 2 km away from the bus bar, respectively; the results are in Table 7.

From Table 7, when S_1 fault occurs with different fault distances, based on step 2, because of $\beta_1 = 2.7267/1.2616 = 2.16 > 2$, step 3 is not needed, and S_1 is selected as the fault line finally. Similarly, based on step 2 when S_4 fault occurs, because of $\beta_2 = 1.6140/1.1455 = 1.41 < 2$, step 3 is needed, since $4.3558 > 3.9845$, and S_4 is selected as the fault line finally. The results show the stepped fault line selection method still applies to the changing fault distances.

8.2. Different Fault Phases. To verify the proposed method adaptability about different fault phases, taking the fault line S_1 and S_4 as examples, the results are as shown in Table 8.

From Table 8, when S_1 fault occurs with different fault phases, based on step 2, because of $\beta_1 = 2.7267/1.2616 = 2.16 > 2$ and $\beta_2 = 2.1819/0.4247 = 5.15 > 2$, step 3 is not needed, and S_1 is selected as the fault line finally. Similarly, based on step 2 when S_4 fault with the changing fault phases, since $\beta_3 = 0.7357/0.6462 = 1.14 < 2$ and $\beta_4 = 3.6244/2.0681 = 1.75 < 2$, step 3 is needed, because of $5.2236 > 3.5225$ and $1.4300 > 1.2483$, and S_4 is selected as the fault line finally. The results show the stepped fault line selection method still applies to the changing fault phases.

8.3. Simulate the Practical Data. Because the conditions of practical environment are poor when fault occurs, therefore, the practical fault data contains much noise. In this paper, in order to analyze the differences between the practical data and the simulation data intuitively, the different intensity noises are injected into the TZSC to simulate the practical data, when SNR is −1.5678 dB and −13.5678 dB, and the results are as shown in Figure 10.

From Figure 10, it can be known that the simulation data can simulate the practical data with the noise background. That is to say, it is possible to verify the proposed algorithm using the practical data. Taking the fault lines S_1 and S_4 as examples, the results are shown in Table 9.

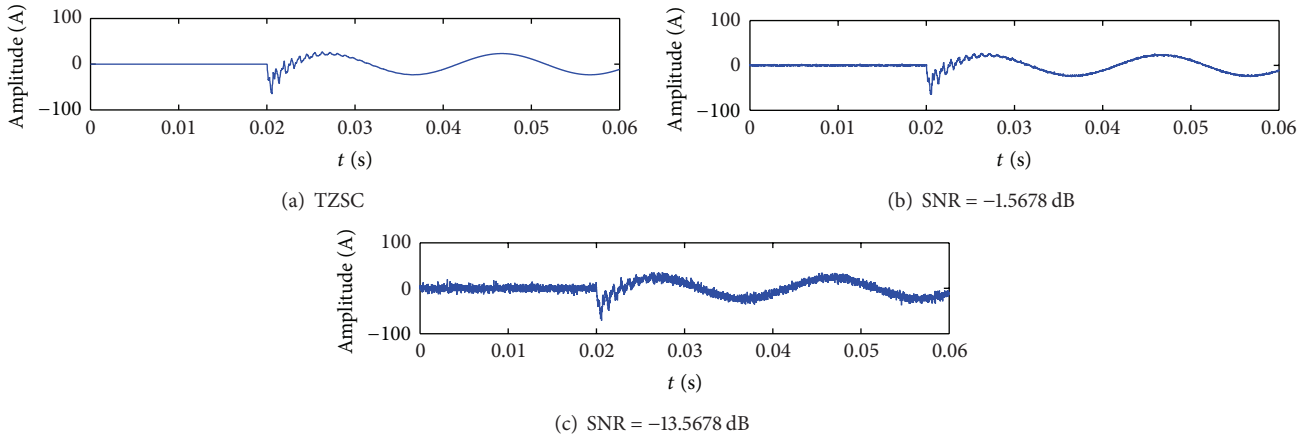

(a) TZSC

(b) SNR = −1.5678 dB

(c) SNR = −13.5678 dB

Figure 10: Simulate the practical fault TZSC.

Table 9: SK relative energy entropy with different intensity noise ($\theta = 0^{\circ}$, $R = 20\,\Omega$).

SNR/dB	Fault line	SK relative energy entropy C_j				Entropy multiple β	Results
		S_1	S_2	S_3	S_4		
−1.5678	Overhead line S_1	3.0665	1.2711	1.3520	2.7091	2.41 > 2	S_1
	Cable line S_4	0.9898	0.8089	4.5347	5.6922	1.22 < 2	S_4
−5.5678	Overhead line S_1	2.9061	1.1725	1.8192	2.7349	2.48 > 2	S_1
	Cable line S_4	0.9375	0.5388	3.7573	5.2826	1.74 < 2	S_4
−10.5678	Overhead line S_1	2.8449	1.0359	1.7698	2.4071	2.75 > 2	S_1
	Cable line S_4	0.8267	0.4481	3.4586	3.9673	1.84 < 2	S_4
−13.5678	Overhead line S_1	2.6814	0.6951	2.0311	2.1538	3.86 > 2	S_1
	Cable line S_4	1.1979	0.7646	4.5726	5.8559	1.57 < 2	S_4

From Table 9, when overhead line S_1 fault occurs, no matter what SNR is equal to, according to steps 1 and 2, $\beta > 2$ establish permanently, step 3 is not needed, and S_1 is selected as the fault line finally. Similarly, when S_4 fault occurs, no matter what SNR is equal to, based on steps 1, 2, and 3, $\beta < 2$ establish all the time, step 3 is needed, since $C_4 > C_3$, and S_4 is selected as fault line finally. It can be seen that the different fault lines can be selected correctly with different intensity noise, and the results show the stepped fault line selection method can apply to the simulative practical fault data.

8.4. Incipient Faults. Compared with the overhead line, the cable line is safer and more economic, so the cable lines are widely used in modern cities. However, the cables are more easily in the state of incipient faults before they fail into permanent faults. Such as the cable line S_4 is in the state of incipient faults in this paper. Usually, incipient faults in power cables gradually result from the aging process, where the localized deterioration in insulation exists. Incipient faults are normally characterized as the faulty phenomena with the relatively small fault currents and the relatively short duration ranging from one-quarter cycle to multicycle. These short lasting current variations cannot be detected by the traditional distribution protection schemes because of their short duration and low increment in magnitude. However, such faults must be detected at the early stage to avoid the consequent catastrophe induced by the degradation themselves [29].

The incipient faults of underground cables are similar to the intermittent arc faults; therefore, the arc model is essential to the analysis of the incipient faults. Paper [30] introduces the arc model; after theoretical analysis and practical verification, arc has nonlinear and time-varying characteristics, and the high-frequency components can be produced. Due to the fact that the arc model is easy, the nonlinear and time-varying characteristics can be expressed, and the arc model is introduced in this paper.

The arc model is built by the energy balance of arc column, and the differential equations of conductivity are used to express

$$\frac{dp}{dt} = \frac{1}{\tau}(P - p), \tag{22}$$

where τ is the time constant of arc, p is the instantaneous conductivity of arc, and P is stable conductivity of arc.

Stable conductivity can be defined as

$$P = \frac{|i_{\text{arc}}|}{u_{\text{st}}}, \quad u_{\text{st}} = u_0 + r_0 \cdot |i_{\text{arc}}|, \tag{23}$$

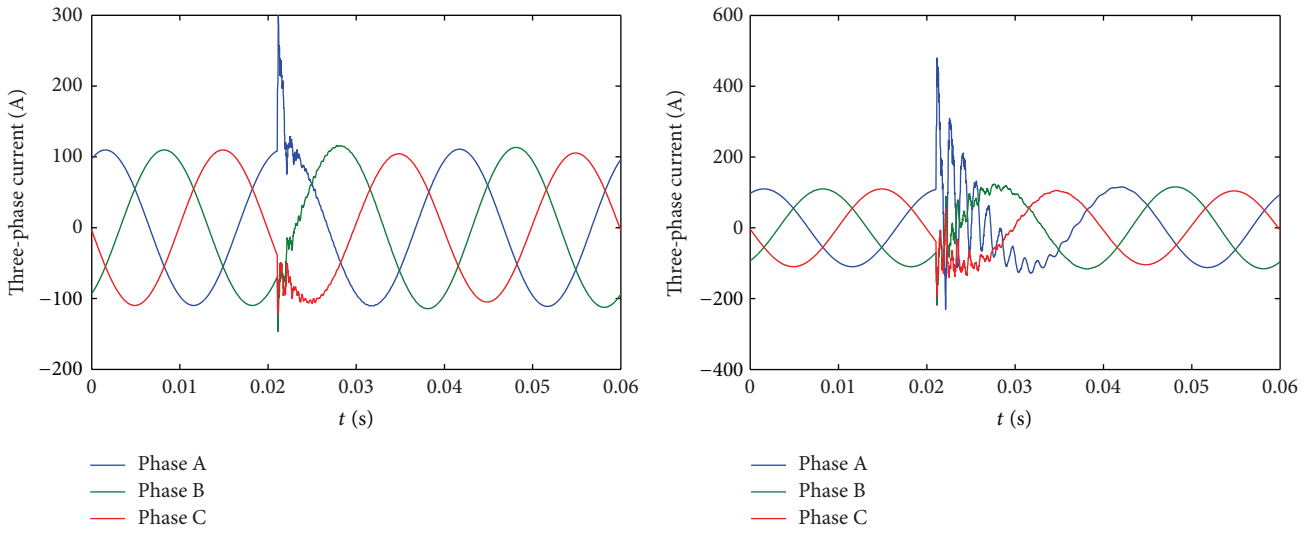

Figure 11: Feeder currents of incipient faults.

Table 10: SK relative energy entropy with incipient faults.

Fault line	θ	R/Ω	SK relative energy entropy C_j				Entropy multiple β	Results
			S_1	S_2	S_3	S_4		
Cable line S_4	0°	1	1.1021	0.6623	4.7252	5.6418	1.66 < 2	S_4
		50	0.3872	0.3602	3.5047	4.1438	1.07 < 2	

where i_{arc} is the instantaneous current of arc, u_{st} is static voltage of arc, u_0 is the voltage characteristics of arc, r_0 is the arc resistance, and the characteristic parameters u_0 and r_0 depend on the length l_{arc} of arc, which can be calculated by

$$u_0 = \left(\frac{0.9l_{arc}}{m} + 0.4\right) \text{kV} \tag{24}$$

$$r_0 = \left(\frac{40l_{arc}}{m} + 8\right) m\Omega. \tag{25}$$

Equation (25) is generalized arc equation. In the resonance grounding system, the parameters of the small current arc change depend on the length of arc, which is the arc elongation *elongspd*. *elongspd* can be defined as

$$elongspd = \frac{dl_{arc}}{dt} = \frac{7l_0}{(0.2v_{th}/v_{max}) + 0.2}, \tag{26}$$

where v_{th} is the instantaneous value of transient initial voltage and v_{max} is the max normal voltage.

The length of arc is defined as a time constant before simulating. The time constant of arc is defined as

$$\tau = \tau_0 \cdot \left(\frac{l_{arc}}{l_0}\right)^{\alpha}, \tag{27}$$

where τ_0 is the initial time constant, l_0 is the initial length of arc, α is the negative coefficient, and the general value of α is -4.

The length of arc is

$$l_{arc} = \left(elongspd \cdot \left(t - t_f\right) + 1\right) \cdot l_0, \tag{28}$$

where t is the simulation time and t_f is the moment that the arc occurs.

In underground cables, the incipient fault is one type of transient, which is prone to an intermittent arc fault. The typical incipient faults are composed of two types: subcycle and multicycle incipient fault. The subcycle incipient fault always occurs near a voltage peak where the arc is ignited, lasts around one-quarter cycle, and self-clears when the current crosses zero. Figure 11(a) shows the three-phase feeder currents when a subcycle incipient fault occurs between phase A to ground. The multicycle incipient fault also likely occurs near a voltage peak, lasts 1–4 cycles, and self-clears when the arc is quenched. The waveforms of the currents are shown in Figure 11(b).

To verify the adaptability of the proposed method when the incipient faults occur, the TZSC of incipient faults is obtained, and then, according to the steps 1, 2, and 3, the selection results are as shown in Table 10.

From Table 10, based on step 2 when S_4 occur incipient faults, it can be known that $\beta_1 = 1.1021/0.6623 = 1.66 < 2$ and $\beta_2 = 0.3872/0.3602 = 1.07 < 2$, step 3 is needed, and since $5.6418 > 4.7252$ and $4.1438 > 3.5047$, S_4 is selected as the fault line finally. The results show that the stepped fault line selection method can also adapt to the incipient faults.

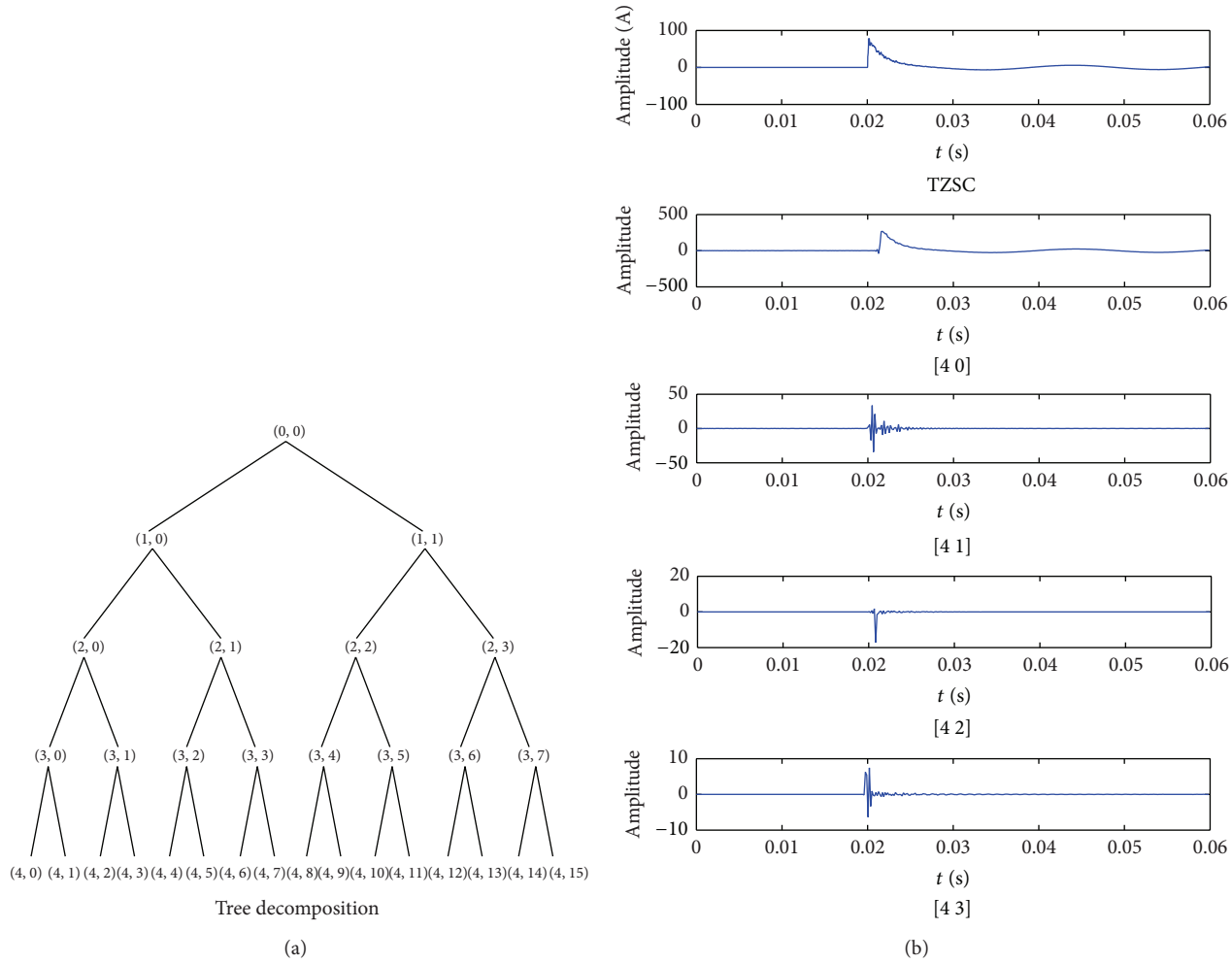

Figure 12: Wavelet decompose the TZSC.

Table 11: Wavelet relative energy entropy.

Fault line	θ	R/Ω	Wavelet relative energy entropy C_j				Entropy multiple β	Results	Right?
			S_1	S_2	S_3	S_4			
Overhead line S_2	0°	20	2.1015	2.4464	2.6801	4.1830	1.16 < 2	S_4	N
		200	1.2593	2.1661	3.6776	3.3619	1.72 < 2	S_3	N
	150°	20	2.1669	2.5476	2.5867	4.4014	1.18 < 2	S_4	N
		200	1.1975	1.9841	3.6561	3.6506	1.66 < 2	S_3	N

9. Compared with Other Fault Line Selection Methods

9.1. Wavelet Relative Energy Entropy. The wavelet mother function "db10" is used to decompose the TZSC [12], and the decomposed layers are 4. Select the frequency bands [4 0], [4 1], [4 2], and [4 3], and the results are shown in Figure 12.

From Figure 12, the lowest frequency band [4 0] is removed, the biggest energy band [4 1] is selected as the characteristic band, because the characteristic band contains the main features of TZSC. And then wavelet denoising and the threshold are used to correct the characteristic band coefficients, successively. Finally, the wavelet relative energy entropies C_j can be obtained, and the selection results are as shown in Table 11.

From Table 11, the method based on wavelet relative energy entropy cannot select the fault line accurately. When the overhead line S_2 fault occurs, according to (21), the entropy multiple β can be calculated, $C_1 > C_2$, while $\beta < 2$ is established, the selection results are incorrectly, because of the big differences on the distribution parameters between the cable line and the overhead line, which make the healthy cable line's entropies bigger than the fault overhead line. Moreover, before the wavelet transform, the appropriate mother wavelet function should be selected, while the selection process is difficult. It can be seen that the accuracy of

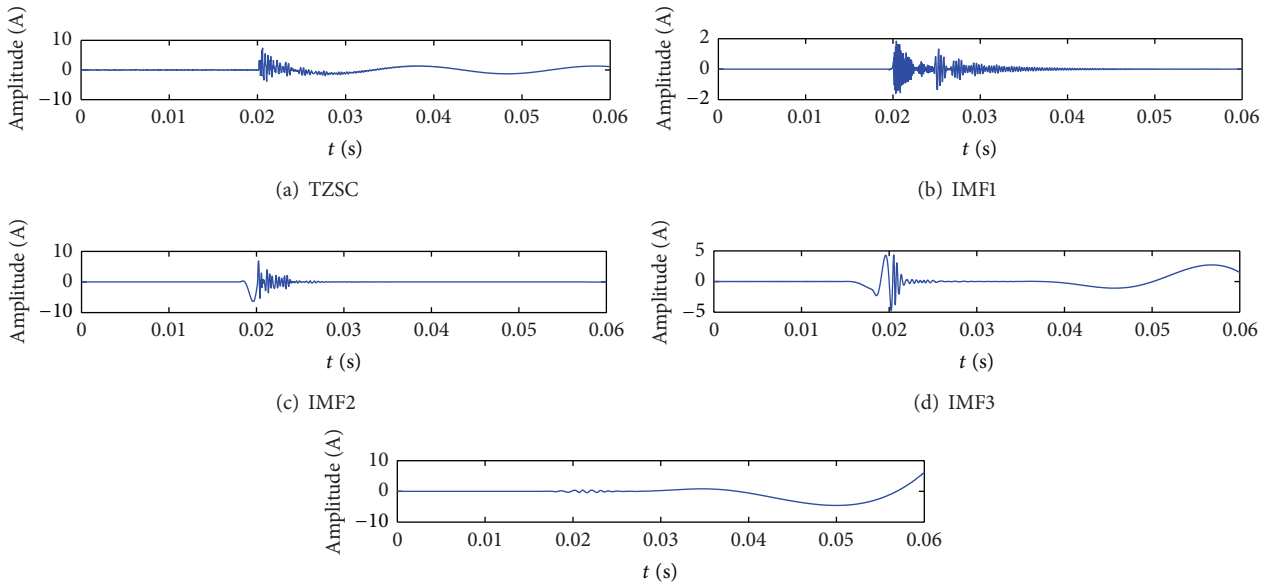

Figure 13: EMD decompose the TZSC.

Table 12: EMD relative energy entropy.

Fault line	θ	R/Ω	EMD relative energy entropy C_j				Entropy multiple β	Results	Right?
			S_1	S_2	S_3	S_4			
Overhead line S_2	0°	20	1.9112	4.5143	5.1857	4.9335	2.36 > 2	S_2	Y
		200	0.8032	3.8554	5.9764	4.8981	4.80 > 2	S_2	Y
	150°	20	2.0273	4.4264	5.7486	4.3812	2.18 > 2	S_2	Y
		200	0.9719	4.1269	6.8780	6.2598	4.25 > 2	S_2	Y
Hybrid line S_3	0°	20	0.7617	1.1209	4.8099	2.8481	1.47 < 2	S_3	Y
		200	0.6714	0.9501	4.7789	2.9695	1.12 < 2	S_3	Y
	150°	20	1.0806	1.5968	5.3013	4.0003	1.48 < 2	S_3	Y
		200	0.7927	1.3501	5.0642	2.7225	1.70 < 2	S_3	Y
Cable line S_4	0°	20	0.5502	0.9428	5.4257	4.2543	1.71 < 2	S_4	Y
		200	0.2029	0.7532	2.0443	3.7942	3.71 > 2	S_2	N
	150°	20	0.2706	0.3861	4.8885	4.0831	1.43 < 2	S_3	N
		200	0.3037	1.5814	4.2905	5.5391	5.21 > 2	S_2	N

the method based on wavelet relative energy entropy is not guaranteed.

9.2. EMD Relative Energy Entropy. The local characteristics of the TZSC can be represented by empirical mode decomposition (EMD); after decomposition, IMF components can be obtained [8], and the waveforms of the mode function IMF1~IMF4 are as shown in Figure 13.

In view of IMF1 component belonging the highest frequency component of the TZSC, containing rich transient information, so IMF1 is selected as the characteristic component, and then wavelet denoising and the threshold are used to correct the characteristic component coefficients. Finally, the relative energy entropies of IMF1 can be obtained, and the selection results are as shown in Table 12.

From Table 12, when the cable line S_4 fault occurs, after decomposition by EMD, the EMD relative energy entropy of each branch line can be obtained, and then the entropy multiple β can be calculated, β is bigger than the threshold, according to steps 1 and 2, the cable line S_4 belongs to the healthy line, and the selection results are incorrect. Moreover, the decomposition process may cause modal aliasing, which can make a big difference on IMF1 component to represent the TZSC. Therefore, it can be seen that the accuracy of the method based on EMD relative energy entropy is not guaranteed.

From Tables 5, 6, 11, and 12, when the branch line fault occurs, because of the big difference of distribution parameters between the cable line and overhead line, the relative energy entropy of each branch line can be obtained, according to the fault line selection steps 1, 2, and 3, and the accuracy

of the method based on wavelet relative energy entropy and EMD relative energy entropy is not guaranteed. Moreover, wavelet transform needs to select the appropriate mother wavelet function, while the selection process is difficult and the modal aliasing may be caused by EMD decomposition process, while SK algorithm can decompose the TZSC in time-frequency domain adaptively, which contributes to the accuracy of the selection results. Therefore, the accuracy of selection method based on SK relative energy entropy is higher than the methods based on the wavelet relative energy entropy and EMD relative energy entropy.

10. Conclusions

This paper proposes a stepped fault line selection method based on SK relative energy entropy, and the conclusions are as follows.

(1) SK belongs to higher order statistics with good ability to restrain the noise and can characterize the TZSC in frequency domain as well. The relative homogeneity of SK energy distribution is described quantitatively by the SK relative energy entropy. In addition, utilizing the max SK relative energy entropy as the criterion to select the fault line, the transient universal characteristic quantity is selected in fact. However, the SK is limited by the compromise problem of time-frequency domain, and the type of window function and the length of window should be determined at the beginning.

(2) The ratios of the first half-wave extremes between neighboring lines and SK relative energy entropy are regarded as fault features to select the fault line. When the bus bar occur fault, the ratios of the first half-wave extreme between neighboring lines are positive. If the entropy multiple is greater than or equal to the threshold, judge the overhead line fault, if not, judge the hybrid line or the cable line fault.

Future work should concentrate on how to determine the appropriate auxiliary noise intensity according to the characteristics of TZSC. Moreover, higher adaptability of the method based on SK relative energy entropy should be advanced with the high resistance.

Notations

HHT: Hilbert-Huang Transform
IMF: Intrinsic mode functions
EMD: Empirical mode decomposition
SK: Spectral kurtosis
TZSC: Transient zero-sequence current
DC: Direct current
STFT: Short-time Fourier transform.

Conflict of Interests

The authors declare that there is no conflict of interests regarding the publication of this paper.

Acknowledgments

This work was supported by the Science and Technology Research (12B470003, 14A470004), the Control Engineering Lab Project (KG2011-15) of Henan Province, China, and the Youth Foundation (Q2012-28, Q2012-43A) of Henan Polytechnic University, China.

References

[1] Z. X. Zhang, X. Liu, and L. Z. Piao, "Fault line detection in neutral point ineffectively grounding power system based on phase-locked loop," *IET Generation , Transmission & Distribution*, vol. 8, no. 2, pp. 273–280, 2014.

[2] M. F. Guo, G. J. Yang, and S. Y. Huang, "Adaptive faulty line selection based on transient characteristics for resonant earthing system," *Electric Power Automation Equipment*, vol. 32, no. 12, pp. 25–31, 2012.

[3] L. Wu, C. Huang, D. Lin, Z. Zhu, and H. Jiang, "Faulty line selection based on transient wavelet energy for non-solid-earthed network," *Electric Power Automation Equipment*, vol. 33, no. 5, pp. 70–75, 2013.

[4] D. Zhou, Z. Liu, F. Hu, and W. Bai, "A new method for fault line selection based on wavelet de-noising and transient current energy grouping comparison in ineffective grounding system," *Power System Protection and Control*, vol. 38, no. 7, pp. 22–28, 2010.

[5] J. Zhang, Z. Y. He, and Y. Jia, "Fault line identification approach based on S-transform," *Proceedings of the CSEE*, vol. 31, no. 10, pp. 109–155, 2011.

[6] H. C. Shu and S. X. Peng, "A fault line detection algorithm for distribution network of overhead line and underground cable mixed lines using S-transform energy from short window data," *Transactions of China Electrotechnical Society*, vol. 24, no. 10, pp. 152–158, 2009.

[7] X. W. Wang, J. W. Wu, and R. Y. Li, "A novel method of fault selection based on voting mechanism of Prony relative entropy theory," *Electric Power*, vol. 46, no. 1, pp. 59–65, 2013.

[8] S. Q. Zhang, X. P. Zhai, and X. Dong, "Application of EMD and Duffing oscillator to fault line detection in un-effectively grounded system," *Proceedings of the CSEE*, vol. 33, no. 10, pp. 161–167, 2013.

[9] H. C. Shu, W. Y. Zhao, and S. X. Peng, "Faulty line selection based on HHT detection for hybrid distribution network," *Electric Power Automation Equipment*, vol. 29, no. 5, pp. 4–10, 2009.

[10] S. Wang and J. F. Zhu, "Faulty line selection of single-phase to ground fault in distribution network based on improved correlation analysis method," *Power System Protection and Control*, vol. 40, no. 15, pp. 76–81, 2012.

[11] H. C. Shu, L. Xu, and S. X. Peng, "An approach for fault feeder line detection in resonant earthed system using correlation analysis," *Electric Power Automation Equipment*, vol. 28, no. 9, pp. 6–9, 2008.

[12] H. C. Shu and S. X. Peng, "Distribution network fault line detection using the full waveband complex relative entropy of wavelet energy," *High Voltage Engineering*, vol. 35, no. 7, pp. 1559–1564, 2009 (Chinese).

[13] F. Immovilli, M. Cocconcelli, A. Bellini, and R. Rubini, "Detection of generalized-roughness bearing fault by spectral-kurtosis energy of vibration or current signals," *IEEE Transactions on Industrial Electronics*, vol. 56, no. 11, pp. 4710–4717, 2009.

[14] F. Millioz and N. Martin, "Circularity of the STFT and spectral kurtosis for time-frequency segmentation in Gaussian environment," *IEEE Transactions on Signal Processing*, vol. 59, no. 2, pp. 515–524, 2011.

[15] H. R. Karimi, P. J. Maralani, B. Lohmann, and B. Moshiri, "H_∞ control of parameter-dependent state-delayed systems using polynomial parameter-dependent quadratic functions," *International Journal of Control*, vol. 78, no. 4, pp. 254–263, 2005.

[16] G. Cheng, Z. G. Liu, and Q. G. Zhang, "Partial discharge signals extraction based on spectral kurtosis," *Electric Power Automation Equipment*, vol. 33, no. 8, pp. 95–110, 2013.

[17] J. Li, T. Y. Jiang, S. Grzybowski, and C. K. Cheng, "Scale dependent wavelet selection for de-noising of partial discharge detection," *IEEE Transactions on Dielectrics and Electrical Insulation*, vol. 17, no. 6, pp. 1705–1714, 2010.

[18] S. Yin, S. X. Ding, A. Haghani, H. Hao, and P. Zhang, "A comparison study of basic data-driven fault diagnosis and process monitoring methods on the benchmark Tennessee Eastman process," *Journal of Process Control*, vol. 22, no. 9, pp. 1567–1581, 2012.

[19] H. R. Karimi, "A computational method for optimal control problem of time-varying state-delayed systems by Haar wavelets," *International Journal of Computer Mathematics*, vol. 83, no. 2, pp. 235–246, 2006.

[20] J. Li, C. Cheng, T. Jiang, and S. Grzybowski, "Wavelet denoising of partial discharge signals based on genetic adaptive threshold estimation," *IEEE Transactions on Dielectrics and Electrical Insulation*, vol. 19, no. 2, pp. 543–549, 2012.

[21] X. N. Kang, X. Liu, J. L. Suonan, C. Ma, C. Wang, and L. Yang, "New method for fault line selection in non-solidly grounded system based on matrix pencil method," *Automation of Electric Power Systems*, vol. 36, no. 12, pp. 88–93, 2012.

[22] S. Yin, H. Luo, and X. Steven, "Real-time implementation of fault-tolerant control systems with performance optimization," *IEEE Transactions on Industrial Electronics*, vol. 61, no. 5, pp. 2402–2411, 2014.

[23] Q. L. Wang and Z. X. Fu, "An adaptive method for single-phase-to-ground fault line selection based on energy entropy measure," *Automation of Electric Power Systems*, vol. 36, no. 5, pp. 103–107, 2012.

[24] H. R. Karimi, "Robust H_∞ filter design for uncertain linear systems over network with network-induced delays and output quantization," *Modeling, Identification and Control*, vol. 30, no. 1, pp. 27–37, 2009.

[25] Q. Q. Jia, L. L. Shi, and N. Wang, "A fusion method for ground fault line detection in compensated power networks based on evidence theory and information entropy," *Transactions of China Electrotechnical Society*, vol. 27, no. 6, pp. 192–197, 2012.

[26] Y. N. Wang, B. I. Huo, and H. Wang, "New criterion for earth fault line selection based on wavelet packets in small current neutral grounding system," *Proceedings of the Chinese Society of Electrical Engineering*, vol. 24, no. 6, pp. 54–58, 2004.

[27] H. R. Karimi, N. A. Duffie, and S. Dashkovskiy, "Local capacity control for production networks of autonomous work systems with time-varying delays," *IEEE Transactions on Automation Science and Engineering*, vol. 7, no. 4, pp. 849–857, 2010.

[28] H. S. Zhang, Z. Y. He, and J. Zhang, "Frequency spectrum characteristic analysis of single-phase grounding fault in resonant grounded systems," *Automation of Electric Power Systems*, vol. 36, no. 6, pp. 79–83, 2012.

[29] T. S. Sidhu and Z.-H. Xu, "Detection of incipient faults in distribution underground cables," *IEEE Transactions on Power Delivery*, vol. 25, no. 3, pp. 1363–1371, 2010.

[30] M. Kizilcay and P. la Seta, "Digital simuimion of fault arcs in medium-voltage distribution networks," in *Proceedings of the 15th Power Systems Computation Conference*, pp. 1–7, 2005.